Real-time imaging of monoclonal antibody film reconstitution after mechanical stress at the air-liquid interface by Brewster angle microscopy

Timotej Žuntar[1], Matjaž Ličen[1], Drago Kuzman[2], and Natan Osterman[1,3,*]

[1]Faculty of Mathematics and Physics, University of Ljubljana, Jadranska 19, Ljubljana, Slovenia

[2]Biologics Drug Product, Technical research and development, Global drug development, Novartis, Lek d.d., Kolodvorska 27, Mengeš, Slovenia

[3]Complex Matter Department, Jožef Stefan Institute, Jamova 39, Ljubljana, Slovenia

*corresponding author

8 Figures (+graphical abstract), 5391 words

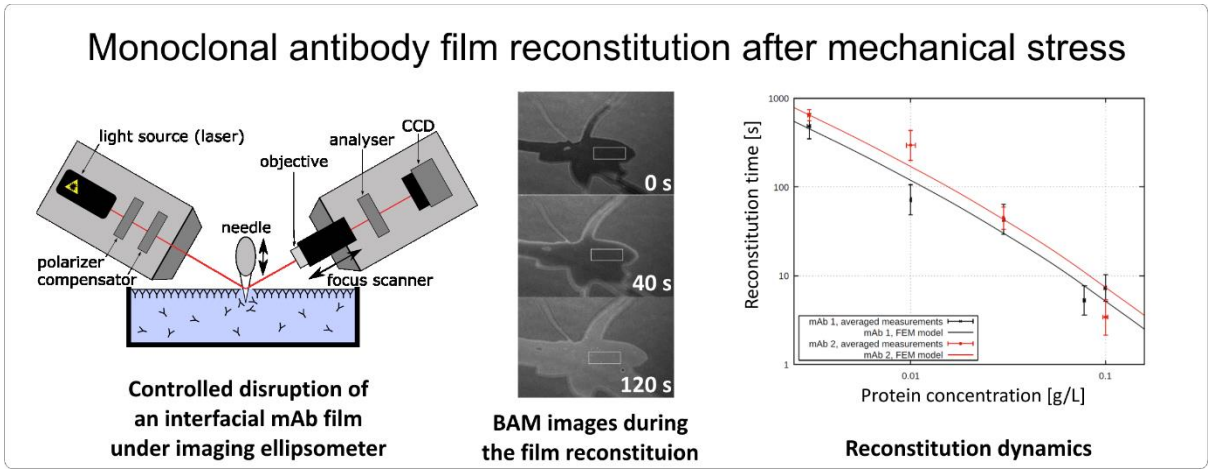

1 Abstract

Monoclonal antibodies (mAbs) represent an important part of biological pharmaceutics. A serious challenge in their development is the formation of protein particles, which are often formed through protein aggregation at the air-liquid interface and then introduced into solution by interfacial stresses. In this paper, protein films formed at the air-liquid interface by two mAbs were disrupted by puncturing them with a microscopic needle, and the subsequent reconstitution of the film was observed in real-time by Brewster angle microscopy. Our results indicate that film reconstitution pace depends on mAb bulk concentration. Numerical modeling gives a quantitative prediction of the surface reconstitution. By extrapolating the model to concentrations typical for pharmaceutical formulations (>30 mg/mL) reconstitution timescales of the protein films can be estimated to be shorter than 0.01 s. Moreover, the effect of polysorbate 80 addition on protein film was studied. Film reconstitution measurements revealed that polysorbate 80 inhibits the film reconstitution process and breaks up the previously formed film.

2 Introduction

Monoclonal antibodies (mAbs) are proteins used as biologic therapeutics to treat a variety of diseases, including cancer, respiratory conditions, autoimmune disorders, and the recently very problematic COVID-19[1–3]. Since mAbs are produced by mammalian cell lines, followed by sophisticated purification steps, and the proteins have inherent instability properties, the development of new mAb drugs is

much more demanding than the development of small-molecule drugs[4]. One such instability is the high tendency of protein molecules to aggregate and form protein particles under a wide range of processing, storage conditions, or shipping[5–7]. Levels of aggregation and particle formation are one of the critical quality attributes of biological drugs with the potential impacts on its efficacy and safety by impairing the biological activity of the drug and by potential induction of immunogenicity or cellular toxicities[8–10]. Since protein molecules have the intrinsic properties to aggregate, particles have been found, at some level, in all commercial therapeutic biological drugs[11]. Therefore, it is essential that the aggregation process is well understood and that levels of aggregates and particles are satisfactorily controlled before such a product can be released to the clinical trial or the market.

Protein particles can generally be formed in a bulk[12] or through protein interactions at interfaces, which in conjunction with interfacial stresses lead to protein denaturation and aggregation[13–20]. While protein molecules come into contact with all manner of interfaces before their eventual application[21], in this paper, we focus on the air-liquid interface, such as the one found, for example, at the top of vials filled with protein formulations.

Proteins often possess amphiphilic properties and consequently form a film at the gas-liquid interface, with their more hydrophobic part oriented towards the gas phase and their more hydrophilic part oriented towards the water phase[22]. It has been demonstrated that interfacial stresses, for example, caused by a stirrer or agitation of the container, cause protein particles to be formed at the interface and introduced into the bulk[19,23–25]. That might be a severe issue for the transport of biologic therapeutics from manufacturer to the patient since biologics are commonly packaged as solutions in vials where a gas-water interface is always present. To combat this problem, surfactants are often added to the solution, covering the interface and preventing protein molecules from aggregation[25–29]; however, surfactants have also been linked to increased protein aggregation in bulk solution[29–33]. In addition, surfactants are prone to enzymatic and chemical hydrolysis, diminishing their protective function and triggering the formation of protein and free fatty acids particles[34].

This paper presents a novel way to study the effects of a controlled disturbance of a protein film. We use a motorized micro-needle to puncture the protein film, creating a small hole in the film, which is then filled with new protein molecules from the bulk solution. The entire process is monitored by Brewster angle microscopy (BAM), providing real-time microscopic images of the film reconstitution process. In BAM, the water surface is illuminated with *p*-polarised light at the Brewster angle for the bulk protein solution. Where the interface is free from surfactants, no light is reflected, resulting in a dark image. However, a protein film at the interface leads to light reflection, resulting in an increased brightness at the detector[35]. The method is widely used to observe interfacial films, including those formed at the surface of protein solutions[26,36–39].

3 Materials and methods

3.1 Sample preparation

Monoclonal antibodies and buffers used in the experiments described in this paper were provided by Lek Pharmaceuticals d.d. (member of Novartis). Monoclonal antibodies were prepared in liquid formulations at 5.3 mg/mL (mAb1) and at 34 mg/mL (mAb2). Both mAbs are known to be susceptible to agitation-induced aggregation.

The samples were prepared by filling syringes with mixtures of appropriate volumes of the above solutions and injecting them into sterile sample tubes through a 0.2 μm filter (Fisherbrand Sterile PES). Subsequently, the samples were deposited employing a pipette into either glass Petri dishes or 35 mm glass-bottomed cell imaging dishes (µ-Dish 35 mm, Ibidi GmbH) and transferred onto the ellipsometer

sample stand; a glass-bottom was used to minimize the amount of scattered light at the detector. Before use, the dishes were cleaned with soap, isopropyl alcohol, and ultrapure water (Milli-Q, Millipore Simplicity) and allowed to dry in a laminar flow cabinet before being exposed to disinfecting UV illumination for several minutes and sealed. Prepared solutions were left undisturbed at the sample stand for at least one hour, allowing for a complete formation of the interfacial film. During this time, we also monitored the film's reflectivity with BAM to ensure that reflectivity was constant before disturbing the film.

In the experiments exploring the effect of surfactants on the reconstitution of the protein film, small quantities of surfactants were slowly deposited into the sample bulk by a micropipette inserted through the air-liquid surface at an angle perpendicular to the laser beam propagation plane to enable continuous imaging.

3.2 Brewster angle microscopy

An Accurion EP3se imaging ellipsometer was used for BAM measurements (**Figure 1**). Sample-air interfaces were illuminated by a 658 nm laser light source operated at 5 mW with the p-polarized reflected component focused through a 10x magnification Nikon objective lens and recorded by a 1392x1040 pixel GigE CCD detector. The incidence angle was chosen to be close to or at Brewster angle (BA) for the sample bulk underneath the interfacial film; in cases where the BA of the bulk could not be verified due to film cover, the angle appropriate for a buffer solution without protein or surfactant additions was chosen. CCD signals averaged over one or more regions of interest were recorded over relevant timescales, along with shorter video recordings of the entire field of view. The sampling frequency varied from approximately 5 to 25 fps due to different exposure times needed to ensure an adequate signal-to-noise ratio.

3.3 Film disruption

A blunt-tipped metal wire of 0.2 mm diameter was inserted to a depth of up to several mm and immediately retracted to disrupt the interfacial film. The insertion angle varied from perpendicular to the interface, which caused smaller disruptions, to slightly diagonal, which enabled the tearing of a larger film area; insertion and retraction speed remained constant in all cases. The wire was actuated by a lever arm affixed to a small stepper motor (28BYJ-48) controlled by an Arduino Nano microcontroller. The assembly was, in turn, connected to a PC from which movement commands were issued manually. For centering the disruption area to the ellipsometer field of view, the stepper assembly was mounted to an XYZ translation stage (Thorlabs PT3/M). The wire-interface distance was gauged by observing surface reflections.

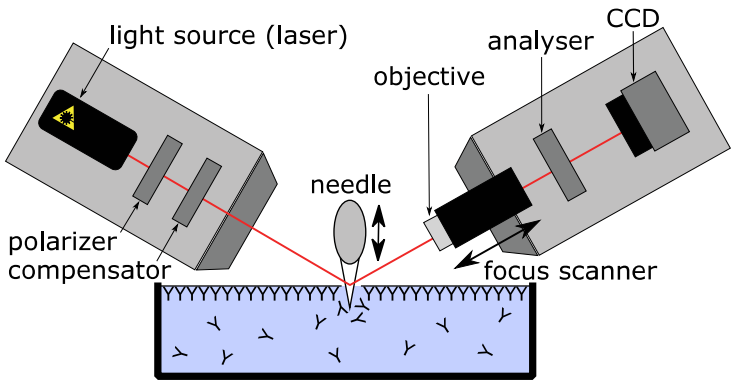

Figure 1: Illustration of the experimental setup. A vertically moving micro-needle punctures the protein film at the air-liquid interface. The subsequent reconstitution of the film is recorded using a Brewster-angle microscope.

3.4 Data analysis

Interface reflectivity vs. time data was obtained by analyzing real-time BAM videos of the liquid-air interface with a custom-developed Python script using the OpenCV and SciPy packages[40]. In each experiment, one or multiple regions of interest (ROIs) were selected within the punctured region of the protein film. Average pixel brightness values in the ROI, proportional to the local interface reflectivity, were then calculated for each frame. In cases of longer timescales where recording the entire field of view would lead to prohibitively large file sizes, a ROI was defined within the ellipsometer control software at the time of puncture, and the averaged brightness vs. time data was extracted automatically. For the purposes of calculating characteristic times of the surface reconstitution process, the data was normalized so that the brightness of the ROI was equal to 1 at the end of the experiment, i.e., when the reflectivity reached an equilibrium value. In addition, the zero of normalized brightness was defined to be the value immediately after the disappearance of the surface ripples generated by the puncture. Characteristic reconstitution times τ were then defined as the time between needle retraction and the normalized ROI brightness reaching an arbitrarily chosen value of 1-1/e = 0.63.

3.5 Numerical model

To model the measured reflectivity changes during film reconstitution, we implemented a simple process of mAb molecule diffusion from the bulk solution to the surface using a commercial finite element method (FEM) package, FEMLAB 3.1 (Comsol Multiphysics). Since the problem has axial symmetry, we implemented it in cylindrical geometry (**Figure 2a**). The disrupted area of film, assumed to be circular with 100 µm radius, was represented by a cylindrical reservoir of varying height with an initial mAb concentration c=0 and a diffusivity value 10 orders of magnitude larger than in the bulk solution, ensuring uniform concentration within the reservoir at all times. 100 µm corresponds to an estimate of the typical dimension of the film area removed by the rupture. A much larger cylinder (400 µm radius, 600 µm height) with a realistic diffusivity constant and an initial mAb concentration c=1 below it represented the bulk solution, with boundary conditions specifying no diffusion through the top surface other than at the reservoir boundary - the already established film - and a constant concentration of 1 elsewhere. Variation of the reservoir height h corresponds to different effective bulk concentrations in the experiment, $h=A/c$, e.g., a two-fold bulk concentration increase is modeled by reducing the reservoir height by a factor of two. Here, A is an unknown proportionality constant that needed to be determined.

Figure 2b shows a typical spatial profile of protein concentration during the film reconstitution process. Molecular concentration in the top reservoir, representing the ruptured region, has risen to 74% of the equilibrium value. While concentration in the bulk region is significantly depleted close to the rupture, it remains nearly undisturbed at a distance of 100 µm.

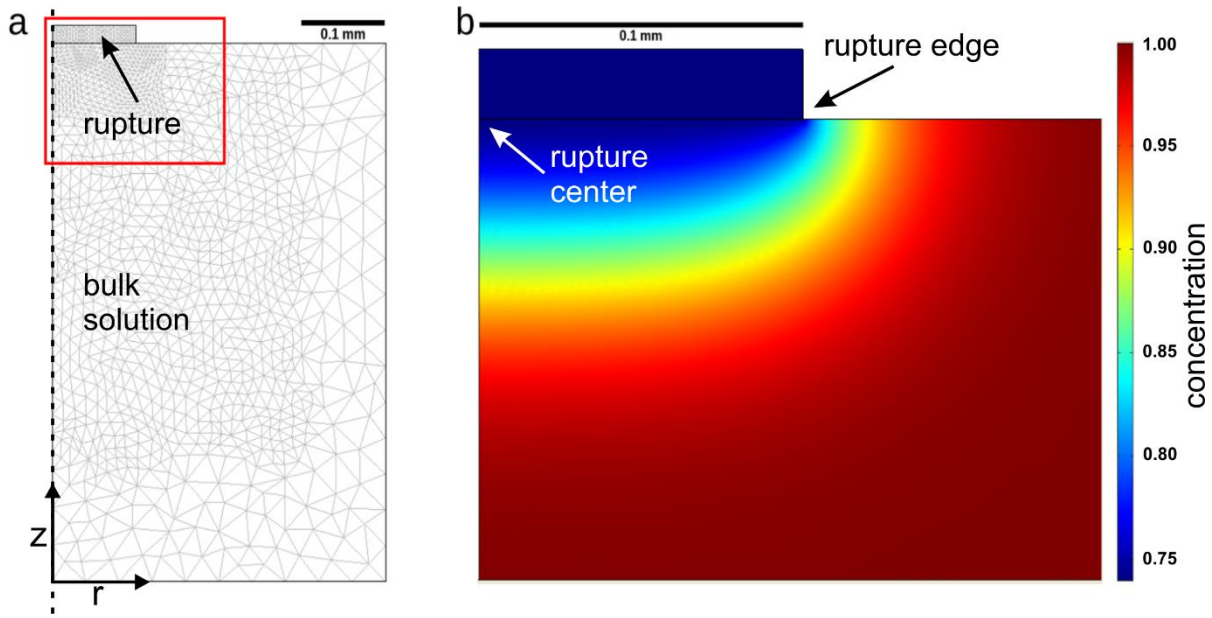

Figure 2: Finite element method modeling of film reconstitution. a) Example of a finite element mesh in 2D cylindrical geometry. A dashed vertical line represents the axis of symmetry. The circular rupture of 100 µm radius is modeled by an initially empty reservoir (c=0) on the top of the bulk solution with an initial concentration of c=1. b) Typical mid-simulation concentration map of the highlighted area in (a). The color bar denotes the protein concentration.

4 Results

4.1 Live observation of mAb film reconstitution after rupture

Both mAb1 and mAb2 formed rigid gel-like films, similar to what has already been reported for proteins in literature[26,41]. Figure 3**a** shows brightness vs. time data for a typical puncture experiment, along with BAM images taken at several points during the experiment. Upon puncturing of the interface, cracks appear in the protein film and begin to fill with protein molecules from the bulk. As the BAM incidence angle is set to the Brewster angle of a clean interface, a non-zero signal on the detector indicates the presence of an interfacial film.

At the start of the experiment, the interface is covered with a uniform film (Figure 3b). Immediately after the puncture of the interface with the needle, there is a short, 2-second transient saturated signal due to capillary waves formed on the surface. Afterward, a hole in the film can be observed (Figure 3c), which begins to gradually fill up with new protein molecules from the bulk (Figure 3d), once again raising the interfacial reflectivity. Eventually, a new equilibrium state is established, and no more change can be observed in the film (Figure 3e). It is apparent that the reflectivity of the reconstituted region of the protein film is higher than in the surrounding area, which was the case in the majority of recorded data, indicating a different molecular packing or different film thickness.

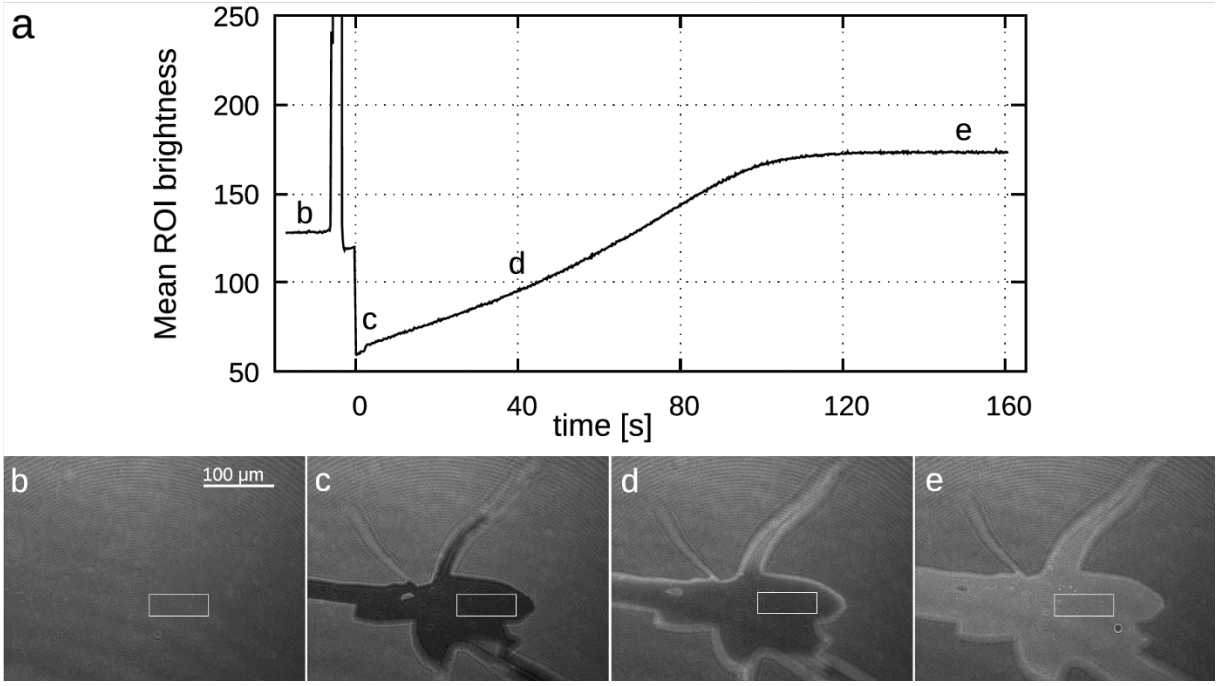

Figure 3: An example of mAb film reconstitution after a disruption event. (a) Raw region of interest (ROI) brightness vs. time data. BAM images of the film at several points during the experiments: (b) before disruption, (c) immediately after disruption, (d) 40 s after disruption, (e) 150 s after disruption. The times when these images were taken are marked in subfigure a. The rectangles in subfigures b-e indicate the ROI which the signal was collected from.

Typical ROI brightness vs. time plots for mAb 1 and mAb 2 films after disruption with a needle for different protein concentrations are shown in Figure 4. For easier comparison, measured reflectivity values are normalized to the final value of reflectivity. As one would expect, reconstitution of the punctured interface with protein molecules occurs faster at higher bulk protein concentrations. However, the reflectivity curves exhibit features which do not match the shapes expected of a purely diffusive process[42], e.g. temporary increases in the rate of brightness increase visible in several of the datasets.

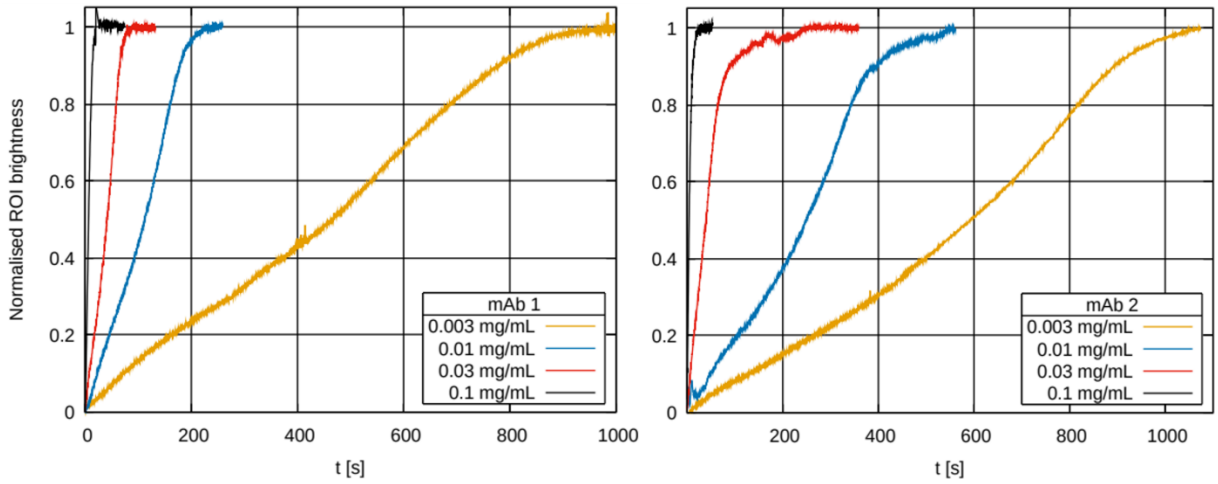

Figure 4: Normalized ROI brightness vs. time in the punctured region measured for different bulk concentrations of mAb 1 (left) and mAb2 (right).

Characteristic times τ of the interfacial reconstitution process for both studied mAbs, obtained from multiple puncture experiments at different bulk protein concentrations, are shown in Figure 5. The data points represent mean values of τ for all experiments conducted at the same concentration c,

with error bars at one standard deviation. To allow for deviations from an ideal diffusive process as a consequence of rupture geometry, convective currents and precursor-mediated adsorption, an empirical power-law expressed as $\tau = Kc^{\alpha}$ was chosen and fitted to the data.

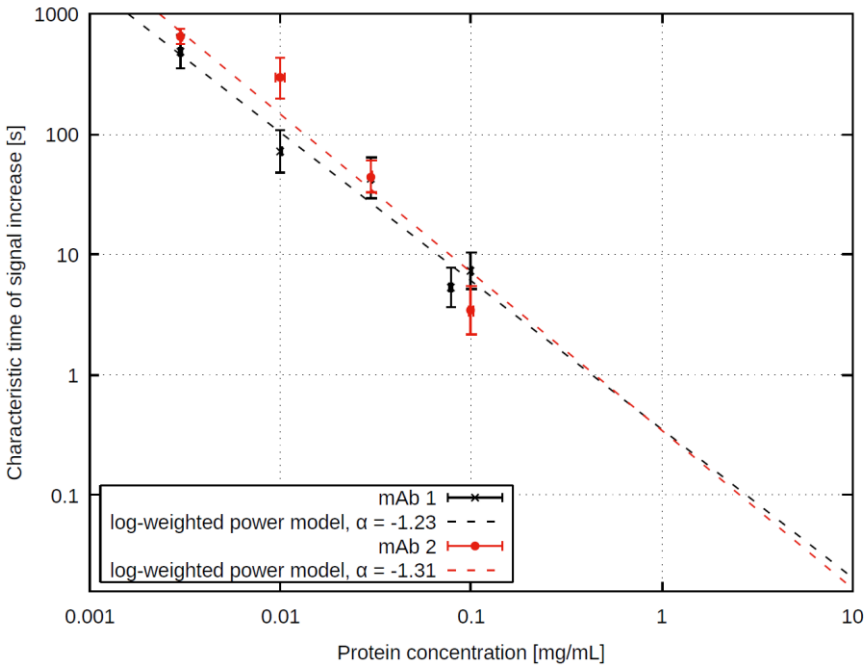

Figure 5: Characteristic times of interface reconstitution for mAb 1 and mAb 2 at different bulk protein concentrations. Dashed lines represent the log-weighted fit of experimental data with the power law, $\tau = Kc^{\alpha}$. The x-axis is extended towards higher concentrations to provide an indication of reconstitution times expected in pharmaceutical formulations under the power law model.

4.2 Numerical modeling of mAb film reconstitution

To account for different bulk mAb concentrations in the experiment, we first ran the FEM simulation for different reservoir heights *h*. For a thin homogeneous layer with smoothly varying refractive index, the intensity of reflected light increases with the square of layer thickness[43]. Therefore, to correlate the experimentally measured changes in brightness with the results of the FEM model, numerically obtained time dependencies of the concentration in the reservoir (representing the ruptured area with no initial film cover) were squared. For each height, we obtained the characteristic rise time τ_c (time to reach the reservoir concentration $c = \sqrt{0.63} = 0.79$ chosen to match the definition of experimentally determined characteristic time as described in Section 3.4), finally acquiring $\tau_c(h)$ dependence. Next, we determined the proportionality constant *A* by fitting $\tau_C(h)$ to the experimentally measured dependence of the characteristic time on the concentration $\tau(c)$.

In Figure 6 we present the modeled dependence of the characteristic time for film reconstitution with the measured values as a function of bulk protein concentration. The values are in good agreement, indicating that even a simple diffusive model is capable of adequately describing the process. Moreover, from the fitted proportionality constant *A* we determined mAb surface density in the adsorbed film: roughly 0.68 ± 0.03 mg/m^2 for mAb 1 and 0.81 ± 0.06 mg/m^2 for mAb 2, which is consistent with the values reported in the literature[44,45].

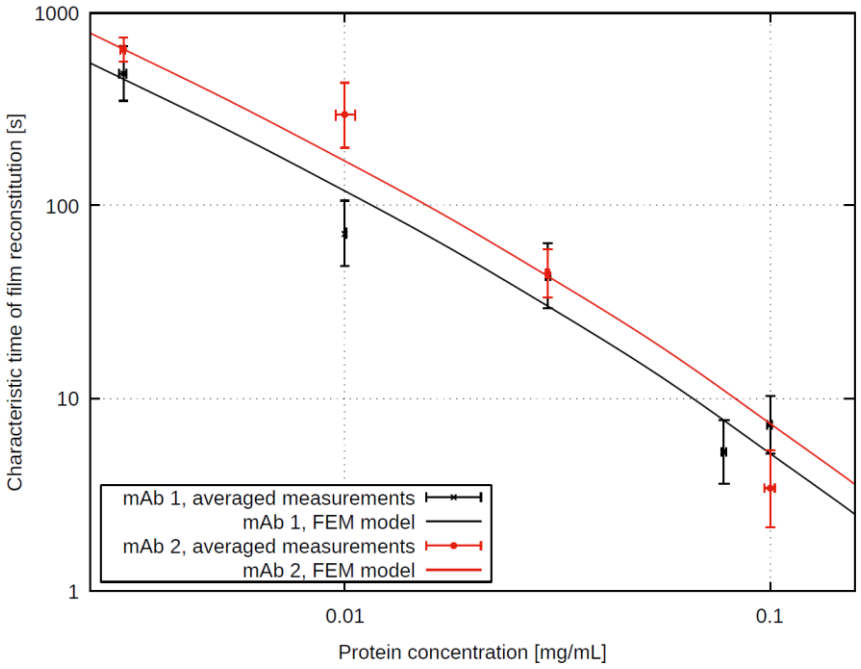

Figure 6: Characteristic time for film reconstitution as a function of bulk protein concentration. Solid lines are FEM model results, and points represent the averaged measurements with error bars at one standard deviation.

4.3 The effect of the surfactant on film reconstitution

It is well known that an addition of surfactants to the protein solution can interfere with the formation of a protein film at air-liquid interfaces. To test how surfactants in the bulk solution affect film reconstitution in puncture experiments, we added different concentrations of PS80 surfactant to a 0.1 mg/mL mAb 1 solution in which an interfacial film had already been established.

Figure7a shows the kinetics of interface reflectivity in the punctured region at different PS80 concentrations. At low bulk PS80 concentration (0.13 µg/mL), reconstitution of the protein film remains essentially unaffected. At moderate PS80 concentrations (0.75 µg/mL), the reconstitution rate slows down, but the film is still eventually re-established (**Figure 7**b). However, when the surfactant concentration is above a critical concentration, the punctured gap is refilled by surfactant molecules, and the protein film never re-forms in the punctured region. This can also be seen in BAM images of the film after transient processes cease: for low to moderate PS80 concentrations, the ruptured region is refilled with protein film (seen as a bright region in **Figure 7**b), while for high PS80 concentrations, the region remains empty (a dark region in **Figure 7**c).

We can assume the critical surfactant concentration for the measured protein concentration to lie between the highest concentration at which film reconstitution was observed and the lowest at which no visible reconstitution occurred, at an order of magnitude of roughly 1 µg/mL (which equals 0.76 µM) at the observed concentrations of both mAbs. This is significantly below the critical micellar concentration of 15 µg/mL (12 µM), reported for PS80. Note that in commercialized biological drugs, the concentration of PS80 is typically in a range 100-200 µg/mL; however, there are some extreme cases as abciximab with 10 µg/mL of PS80 and dupilimumab with 2000 µg/mL [46].

While sufficiently high concentrations of PS80 prevented the formation of new protein film at the air-liquid interface, they did not immediately remove the existing film. After multiple days, the film was still observable; however, the film morphology observed in BAM images suggests that surfactant molecules are slowly integrated into the film (**Figure 8**)[26,47–49].

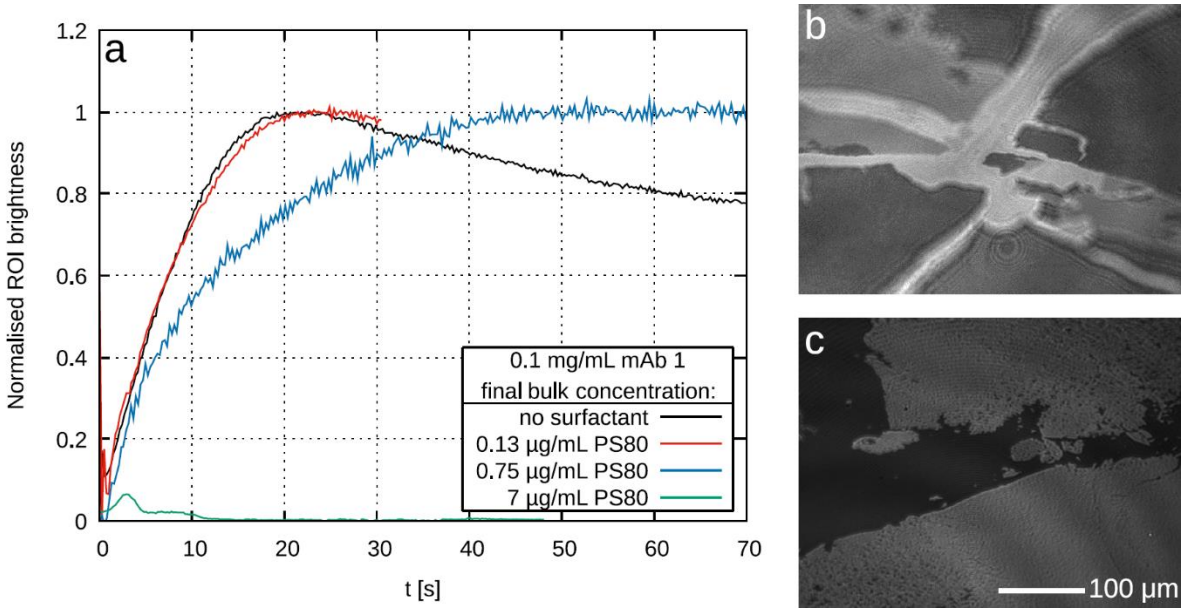

Figure 7: The effect of the surfactant on the film reconstitution after puncture. (a) Representative normalized ROI brightness vs. time curves of ruptured regions in the interfacial film of a 0.1 mg/mL mAb 1 solution with different concentrations of added PS80 surfactant. (b, c) BAM images of the interfacial rupture after a long time at PS80 concentrations of: (b) 0.13 µg/mL, and (c) 7 µg/mL.

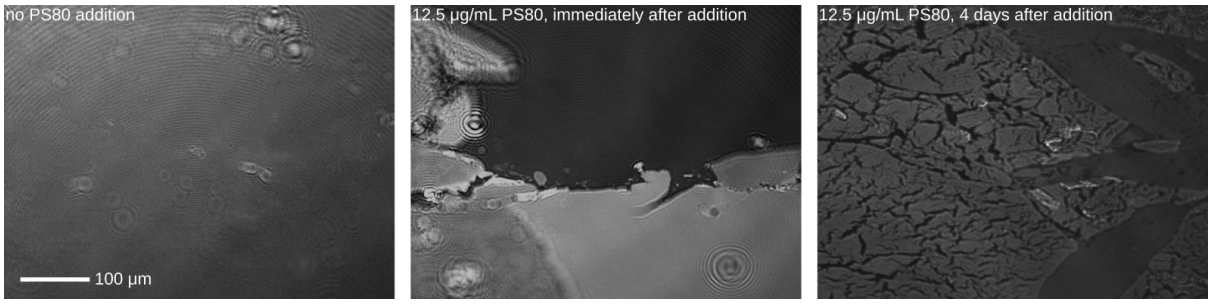

Figure 8: The effect of surfactant addition on the undisturbed interfacial film: (left) surface of a 0.03 mg/mL mAb 1 solution after initial film formation, (center) immediately after the addition of undiluted PS80 bringing the total surfactant concentration to 12.5 µg/mL and (right) after four days. The images do not represent the same area of the sample surface.

5 Discussion

The characteristic times for reconstitution of the film surface were relatively short compared to characteristic times for protein film formation available in literature obtained by measurements of surface pressure[14,22]. However, they agree with the times extracted from optical observations of the formation of interfacial mAb film by Kannan *et al*[14]. The authors also noted that optical measurements result in much shorter characteristic times than measurements of surface pressure. This could be attributed to surface pressure measurements being more sensitive to changes in protein molecular structure, such as unfolding and aggregation at the air-liquid interface, while reflectance depends mainly on the macroscopic properties of the film. In fact, in light of recent research it is likely that a slower reorientation process is taking place well after the reflectivity has reached an equilibrium value and the measured data only correspond to the initial stage of adsorption[50]. However, the experimental setup was poorly suited for longer observations and the possibility could not be tested.

The data presented in Figure 6 suggests that the characteristic time-concentration relationship for mAbs can be roughly described with a power law. The same functional dependence is also obtained in the FEM simulation, indicating that slow diffusion of protein molecules towards the interface is the limiting factor for film reconstitution. However, other factors influence reconstitution dynamics, such as the possibility of convective currents caused by the rapid movement of the puncturing wire and conformational changes in the existing protein network, possibly influencing further adsorption. An extrapolation to concentrations typically found in pharmaceutical protein formulations yields a characteristic reconstitution time on the order of 10 ms at 10 mg/mL and 1 ms at 100 mg/mL. Due to the limitations of the chosen observation method, behavior in this range of mAb concentrations could not be experimentally verified as the film re-formed at a timescale comparable with transient effects due to the puncture caused by surface tension. Another limiting factor is the frame rate of the camera. On the other hand, reconstitution at lower concentrations is slow enough for evaporation to alter the position of the interface significantly, and with it, the path of the reflected light beam, eventually departing the camera field of view altogether. Covering the samples during measurements was not feasible as it significantly degraded the signal.

Careful observation of film re-formation in the ruptured area reveals that the reconstitution is fastest near the rupture edges. This can be seen in **Figures 3**c, d, and e, where thin cracks in the interfacial film and the edge of the rupture are already bright after 40 s, whereas the rupture is still dark, indicating that film has not yet fully reconstituted. This observation agrees with the diffusive model: protein molecules that adsorb to a film-free surface far away from other film edges can originate just from below, whereas molecules that adsorb close to the existing film can originate either directly from below as well as from any adjacent area below the film.The situation can be nicely seen in the simulated concentration map (**Figure 2**b)**:** the closest point of nearly non-depleted protein concentration (c=0.99) lies approximately 100 µm below the center of the ruptured region (at r=0), whereas the closest point of such concentration for the edge of the rupture (at r=100 µm) lies sideways, just 50 µm away in the horizontal direction. While no migration of protein from the surrounding film into the rupture is possible in the model, this condition also seems to hold true for experiments, as indicated by continuously well defined rupture boundaries.

We have also performed similar puncture/reconstitution experiments on protein films with lower rigidity, where lateral diffusion into a rupture from the surrounding film is apparent. However, convection currents on both sides of the interface, partially caused by localized heating by the ellipsometer beam, caused a drift of the adsorbed film, which required either dynamical adjustment of the ROI or physical movement of the sample in the case of larger drifts. The latter approach yielded poor results due to mechanical disturbances caused by the movement.

The purpose of surfactant addition to pharmaceutical formulations is the complete coverage of the interface with surfactant molecules to prevent protein adsorption and consequently reduce the agitation-induced formation of undesired protein particles from the mAb film. We have quantitatively demonstrated that the addition of the surfactant significantly alters the film reconstitution process. However, the surfactant had an immediate effect only in the regions where the protein film was removed.It did not completely remove the existing protein film, which is consistent with reports in the literature[26].

6 Conclusions

We have presented a first real-time microscopic optical observation of re-formation of a ruptured mAb film. The obtained characteristic times indicate that the reconstitution of films formed at the air-liquid interface of protein solutions with concentrations typical for pharmaceutical protein formulations occurs on time scales much shorter than 1 s. This is an important factor in the context of unwanted protein aggregation and the formation of insoluble protein particles during production and shipping of biological drugs. Whenever the interfacial layer is under mechanical stress (by puncturing in our experiment, agitation during the production, or shaking during transport), the film ruptures, and pieces of it end up in the bulk solution in the form of undesired sub-visible protein particles. We have shown that the protein film is re-formed in a fraction of a second under these conditions and thus ready for another generation of particles during the next disruption.

The addition of surfactant to the solution does not remove already established mAb films at the air-solution interface. After puncturing the film, however, the surfactant competitively adsorbs onto the interface, slowing down the film reconstitution. Sufficiently high surfactant concentration completely prevents the process.

The developed finite element model provides a quantitative prediction of surface reconstitution. The simulation reproduced the experimental findings remarkably well, indicating that diffusion adequately describes the process.

Given the ease of implementing the puncturing experiment on commercially available ellipsometers, we anticipate that such measurement could be widely employed to study the mode of action of different surfactants at the air/liquid interface and to rapidly optimize the type and concentration of surfactant used in drug products with minimal material requirements. In contrast to the traditional determination of surfactant concentration through long-term agitation experiments and subsequent analysis of formed aggregates, the puncturing experiment provides immediate results.

We thank Lek, d.d. for financial support and supply of the materials used in this work. N.O. acknowledges financial support from the Slovenian Research Agency (Research Core Funding No. P1-0192).

7 Bibliography

1. Leader, B., Baca, Q. J. & Golan, D. E. Protein therapeutics: a summary and pharmacological classification. *Nat. Rev. Drug Discov.* **7**, 21–39 (2008).
2. Weiner, L. M., Surana, R. & Wang, S. Monoclonal antibodies: versatile platforms for cancer immunotherapy. *Nat. Rev. Immunol.* **10**, 317–327 (2010).
3. What is bamlanivimab | Antibody Drug | Lilly COVID-19 Treatment. https://www.covid19.lilly.com/bamlanivimab.
4. Lagassé, H. A. D. *et al.* Recent advances in (therapeutic protein) drug development. *F1000Research* **6**, (2017).
5. *Aggregation of therapeutic proteins*. (Wiley, 2010).
6. Wang, W. & Roberts, C. J. Protein aggregation - Mechanisms, detection, and control. *Int. J. Pharm.* **550**, 251–268 (2018).

7. Nicoud, L., Owczarz, M., Arosio, P. & Morbidelli, M. A multiscale view of therapeutic protein aggregation: A colloid science perspective. *Biotechnol. J.* **10**, 367–378 (2015).

8. Wang, W. *et al.* Immunogenicity of protein aggregates--concerns and realities. *Int. J. Pharm.* **431**, 1–11 (2012).

9. Moussa, E. M. *et al.* Immunogenicity of Therapeutic Protein Aggregates. *J. Pharm. Sci.* **105**, 417–430 (2016).

10. Roberts, C. J. Protein aggregation and its impact on product quality. *Curr. Opin. Biotechnol.* **30**, 211–217 (2014).

11. Singh, S. K. *et al.* An industry perspective on the monitoring of subvisible particles as a quality attribute for protein therapeutics. *J. Pharm. Sci.* **99**, 3302–3321 (2010).

12. Zidar, M., Posnjak, G., Muševič, I., Ravnik, M. & Kuzman, D. Surfaces Affect Screening Reliability in Formulation Development of Biologics. *Pharm. Res.* **37**, 27 (2020).

13. Li, J. *et al.* Interfacial Stress in the Development of Biologics: Fundamental Understanding, Current Practice, and Future Perspective. *AAPS J.* **21**, 44 (2019).

14. Kannan, A., Shieh, I. C. & Fuller, G. G. Linking aggregation and interfacial properties in monoclonal antibody-surfactant formulations. *J. Colloid Interface Sci.* **550**, 128–138 (2019).

15. Sorret, L. L., DeWinter, M. A., Schwartz, D. K. & Randolph, T. W. Protein-protein interactions controlling interfacial aggregation of rhIL-1ra are not described by simple colloid models: Protein Aggregation at Interfaces. *Protein Sci.* **27**, 1191–1204 (2018).

16. Koepf, E., Eisele, S., Schroeder, R., Brezesinski, G. & Friess, W. Notorious but not understood: How liquid-air interfacial stress triggers protein aggregation. *Int. J. Pharm.* **537**, 202–212 (2018).

17. Ghazvini, S., Kalonia, C., Volkin, D. B. & Dhar, P. Evaluating the Role of the Air-Solution Interface on the Mechanism of Subvisible Particle Formation Caused by Mechanical Agitation for an IgG1 mAb. *J. Pharm. Sci.* **105**, 1643–1656 (2016).

18. Mehta, S. B., Lewus, R., Bee, J. S., Randolph, T. W. & Carpenter, J. F. Gelation of a Monoclonal Antibody at the Silicone Oil–Water Interface and Subsequent Rupture of the Interfacial Gel Results in Aggregation and Particle Formation. *J. Pharm. Sci.* **104**, 1282–1290 (2015).

19. Wiesbauer, J., Prassl, R. & Nidetzky, B. Renewal of the Air–Water Interface as a Critical System Parameter of Protein Stability: Aggregation of the Human Growth Hormone and Its Prevention by Surface-Active Compounds. *Langmuir* **29**, 15240–15250 (2013).

20. Duerkop, M., Berger, E., Dürauer, A. & Jungbauer, A. Impact of Cavitation, High Shear Stress and Air/Liquid Interfaces on Protein Aggregation. *Biotechnol. J.* **13**, 1800062 (2018).

21. Bee, J. S., Randolph, T. W., Carpenter, J. F., Bishop, S. M. & Dimitrova, M. N. Effects of surfaces and leachables on the stability of biopharmaceuticals. *J. Pharm. Sci.* **100**, 4158–4170 (2011).

22. Koepf, E., Schroeder, R., Brezesinski, G. & Friess, W. The film tells the story: Physical-chemical characteristics of IgG at the liquid-air interface. *Eur. J. Pharm. Biopharm.* **119**, 396–407 (2017).

23. Kiese, S., Papppenberger, A., Friess, W. & Mahler, H.-C. Shaken, Not Stirred: Mechanical Stress Testing of an IgG1 Antibody. *J. Pharm. Sci.* **97**, 4347–4366 (2008).

24. Bee, J. S. *et al.* Production of particles of therapeutic proteins at the air–water interface during compression/dilation cycles. *Soft Matter* **8**, 10329–10335 (2012).

25. Rudiuk, S., Cohen-Tannoudji, L., Huille, S. & Tribet, C. Importance of the dynamics of adsorption and of a transient interfacial stress on the formation of aggregates of IgG antibodies. *Soft Matter* **8**, 2651–2661 (2012).

26. Rabe, M., Kerth, A., Blume, A. & Garidel, P. Albumin displacement at the air–water interface by Tween (Polysorbate) surfactants. *Eur. Biophys. J.* **49**, 533–547 (2020).

27. Kannan, A., Shieh, I. C., Leiske, D. L. & Fuller, G. G. Monoclonal Antibody Interfaces: Dilatation Mechanics and Bubble Coalescence. *Langmuir* **34**, 630–638 (2018).

28. Khan, T. A., Mahler, H.-C. & Kishore, R. S. K. Key interactions of [NONIONIC] surfactants in therapeutic protein formulations: A review. *Eur. J. Pharm. Biopharm.* **97**, 60–67 (2015).

29. Serno, T., Carpenter, J. F., Randolph, T. W. & Winter, G. Inhibition of agitation-induced aggregation of an IgG-antibody by hydroxypropyl-beta-cyclodextrin. *J. Pharm. Sci.* **99**, 1193–1206 (2010).

30. Liu, L., Qi, W., Schwartz, D. K., Randolph, T. W. & Carpenter, J. F. The Effects of Excipients on Protein Aggregation During Agitation: An Interfacial Shear Rheology Study. *J Pharm Sci* **102**, 2460–2470 (2013).

31. Ismael, M. A. Unraveling the molecular mechanism of the effects of sodium dodecyl sulfate, salts, and sugars on amyloid fibril formation in camel IgG. 8 (2018).

32. Wang, W., Wang, Y. J. & Wang, D. Q. Dual effects of Tween 80 on protein stability. *Int. J. Pharm.* **347**, 31–38 (2008).

33. Larson, N. R. *et al.* Comparison of Polysorbate 80 Hydrolysis and Oxidation on the Aggregation of a Monoclonal Antibody. *J. Pharm. Sci.* **109**, 633–639 (2020).

34. Roy, I. *et al.* Polysorbate Degradation and Particle Formation in a High Concentration mAb: Formulation Strategies to Minimize Effect of Enzymatic Polysorbate Degradation. *J. Pharm. Sci.* **110**, 3313–3323 (2021).

35. Vollhardt, D. Brewster angle microscopy: A preferential method for mesoscopic characterization of monolayers at the air/water interface. *Curr. Opin. Colloid Interface Sci.* **19**, 183–197 (2014).

36. Sakai, A. *et al.* Interaction of Trastuzumab with biomembrane models at air-water interfaces mimicking cancer cell surfaces. *Biochim. Biophys. Acta BBA - Biomembr.* **1861**, 182992 (2019).

37. Rodríguez Niño, M. R., Sánchez, C. C., Ruíz-Henestrosa, V. P. & Patino, J. M. R. Milk and soy protein films at the air–water interface. *Food Hydrocoll.* **19**, 417–428 (2005).

38. Lipp, M. M., Lee, K. Y., Waring, A. & Zasadzinski, J. A. Fluorescence, polarized fluorescence, and Brewster angle microscopy of palmitic acid and lung surfactant protein B monolayers. *Biophys. J.* **72**, 22 (1997).

39. Murray, B. S., Xu, R. & Dickinson, E. Brewster angle microscopy of adsorbed protein films at air–water and oil–water interfaces after compression, expansion and heat processing. *Food Hydrocoll.* **23**, 1190–1197 (2009).

40. SciPy 1.0 Contributors *et al.* SciPy 1.0: fundamental algorithms for scientific computing in Python. *Nat. Methods* **17**, 261–272 (2020).

41. Mackie, A. R., Gunning, A. P., Wilde, P. J. & Morris, V. J. Orogenic Displacement of Protein from the Air/Water Interface by Competitive Adsorption. *J. Colloid Interface Sci.* **210**, 157–166 (1999).

42. Fernsler, J. G. & Zasadzinski, J. A. Competitive Adsorption: A Physical Model for Lung Surfactant Inactivation. *Langmuir ACS J. Surf. Colloids* **25**, 8131–8143 (2009).

43. Winsel, K., H�nig, D., Lunkenheimer, K., Geggel, K. & Witt, C. Quantitative Brewster angle microscopy of the surface film of human broncho-alveolar lavage fluid. *Eur. Biophys. J.* **32**, 544–552 (2003).

44. Hollowell, P. *et al.* Recent Advances in Studying Interfacial Adsorption of Bioengineered Monoclonal Antibodies. *Molecules* **25**, 2047 (2020).

45. Kanthe, A. D. *et al.* Armoring the Interface with Surfactants to Prevent the Adsorption of Monoclonal Antibodies. *ACS Appl. Mater. Interfaces* **12**, 9977–9988 (2020).

46. Strickley, R. G. & Lambert, W. J. A review of Formulations of Commercially Available Antibodies. *J. Pharm. Sci.* **110**, 2590-2608.e56 (2021).

47. Mackie, A. & Wilde, P. The role of interactions in defining the structure of mixed protein–surfactant interfaces. *Adv. Colloid Interface Sci.* **117**, 3–13 (2005).

48. Rodríguez Patino, J. M., Rodríguez Niño, Ma. R. & Carrera Sánchez, C. Physico-chemical properties of surfactant and protein films. *Curr. Opin. Colloid Interface Sci.* **12**, 187–195 (2007).

49. Gunning, P. A. *et al.* The effect of surfactant type on protein displacement from the air–water interface. *Food Hydrocoll.* **18**, 509–515 (2004).

50. Kanthe, A. *et al.* No ordinary proteins: Adsorption and molecular orientation of monoclonal antibodies. *Sci. Adv.* **7**, eabg2873 (2021).